

On temporal entropy and the complexity of computing the expectation value of local operators after a quench.

Stefano Carignano,¹ Carlos Ramos Marimón,² and Luca Tagliacozzo³

¹Barcelona Supercomputing Center*

²Departament de Física Quàntica i Astrofísica and Institut de Ciències del Cosmos (ICCUB),

Universitat de Barcelona, Martí i Franquès 1, 08028 Barcelona, Catalonia, Spain

³Institute of Fundamental Physics IFF-CSIC, Calle Serrano 113b, Madrid 28006, Spain†

We study the computational complexity of simulating the time-dependent expectation value of a local operator in a one-dimensional quantum system by using temporal matrix product states. We argue that such cost is intimately related to that of encoding temporal transition matrices and their partial traces. In particular, we show that we can upper-bound the rank of these reduced transition matrices by the one of the Heisenberg evolution of local operators, thus making connection between two apparently different quantities, the temporal entanglement and the local operator entanglement. As a result, whenever the local operator entanglement grows slower than linearly in time, we show that computing time-dependent expectation values of local operators using temporal matrix product states is likely advantageous with respect to computing the same quantities using standard matrix product states techniques.

Introduction. The complexity of simulating quantum-many body systems increases exponentially with the number of its constituents. As a result, we still cannot understand from first principles important physical mechanisms, such as the origin of high-temperature superconductivity. Over the last decades, the development of tensor networks techniques has however helped in gaining better insight on the equilibrium properties of many-body quantum systems. It is now understood that, at equilibrium, quantum complexity is mostly related to the amount of entanglement contained in many-body quantum systems, and we have been able to design tensor network Ansätze that can cope with the entanglement present in typical equilibrium states. This has led to important advances, and while we still don't have final answers about the origin of high-temperature superconductivity, we now know much more about the phase diagram of the Hubbard model, one of the prime candidates to describe it [1].

Out of equilibrium, the situation is different: even in the simplest protocol, such as e.g. quantum quenches, time evolution quickly produces robustly entangled states, with correlations spreading over large distances [2]. Standard tensor network techniques such as those based on matrix product states (MPS) thus struggle to cope with the fast growth of entanglement and, as a result, their cost increases exponentially with the duration of the evolution [3].

This fact is a consequence of trying to represent the full quantum state during the evolution. A legitimate question that has been asked in the last few years, is whether the situation changes if one gives up on the full description of the state and focuses rather on a local description, by trying to correctly describe the evolution of the expectation value of local operators. In principle, this is a much simpler task, even though it is not clear how to systematically rephrase the Hamiltonian evolution of the

full state to a dissipative evolution of one of its subsystems. Several approaches however have been proposed, with partial success in specific cases, see e.g. Refs. [4–12]. However, except for few studies on integrable systems [13, 14], there has been no systematic understanding of the real computational cost of such approaches and thus no concrete understanding on the complexity of simulating the evolution of local observables.

In this work we make a first step in this direction. We consider the evolution under a local Hamiltonian of the expectation value of a local observable and define a slightly modified version of the algorithms introduced by Bañuls and collaborators in 2009 [4], following the inspirational papers [5, 6, 10, 12]. These algorithms rely still on a matrix product state, which is however now defined in time, making it a temporal MPS (tMPS) along a Keldysh contour [6, 15]. It has recently been noticed that such tMPS encodes the influence matrix of the system [16] that drives the evolution of a region of the full system, and thus provides the systematic way of translating the global evolution into a local one [11, 17, 18]. Furthermore, it was found that in specific cases, such tMPS can be described with small bond dimension. Other cases were reported where on the other hand this was not the case [4, 5].

Here we provide some theoretical backup to these numerical observations, trying to identify scenarios when the use of tMPS provides an efficient algorithm to predict the out-of-equilibrium dynamics of local observables. Our main result in this direction is to relate the complexity of the tMPS with the one of encoding the time evolution of operators in the Heisenberg picture.

Such complexity is encoded in the so called “operator entanglement” [19, 20], which has already been used as a measure to distinguish easy-to-simulate from hard-to-simulate systems. In particular, the authors of those papers claim that the operator entanglement grows at most

logarithmically in time for integrable systems, whereas it increases linearly for non-integrable systems. Such a claim has been verified by several other authors, see e.g. Refs [21–23].

Our result here is to show that a small modification of the standard tMPS algorithms allows to make direct contact between the behaviour of the operator entanglement and the rank of the tMPS. In particular, whenever the operator entanglement grows logarithmically in time, we can show that the tMPS bond dimension is bounded by a polynomial growth in time. On the other hand, whenever the operator entanglement grows linearly in time, our bound on the tMPS bond dimension is exponential. This does not rule out that there might be specific cases in which the tMPS might still have a small bond dimension, but we believe that in the generic case this should not happen. We indeed provide scenarios in which such bound is saturated along the line of the examples presented previously [10].

As a result, if the conjectured different growth of the operator entanglement for integrable and generic systems is correct, our results can be used to show that only in the case of integrable systems the rank of the tMPS matrices can be safely upper bounded by a polynomial growth in time.

Setup. Given a lattice system, we consider the complexity of computing the evolution of the expectation value of a local operator after a quench. We start from a product state $|\psi_0\rangle$ and a local Hamiltonian H . The system starts to evolve and it is described by the state $|\psi(T)\rangle = \exp(-iHT)|\psi_0\rangle \equiv U(T)|\psi_0\rangle$. In general, the entanglement entropy of the state increases linearly in time [2] and standard time-dependent MPS simulations become exponentially expensive [24, 25] (for recent reviews see also [26, 27]). Here, rather than evolving the state, we focus on the evolution of the expectation value of a local operator acting on two neighbouring sites [28],

$$\langle \mathcal{O}\mathcal{Q} \rangle(T) = \langle \psi(T) | \mathcal{O}_i \mathcal{Q}_{i+1} | \psi(T) \rangle. \quad (1)$$

Approximating $U(T)$ by a sequence of short evolutions $U(\delta t)^{N_T}$ with $N_T = T/\delta t$ and using a Trotter expansion, this quantity is encoded in the contraction of a two dimensional TN containing order $N_x \times N_T$ tensors [29, 30], as shown in Fig. 1(a). Furthermore, one can fold the network following [4, 5], leading to a double-layer structure as shown in Fig. 1 (b).

Being two-dimensional, the best contraction path for this tensor network is not a priori obvious. We can nevertheless make use of an important simplification originating in the Trotter approximation, namely that the time evolution of a local operator has an exact causal cone obtained by cancelling all the unitary gates that are contracted with their respective Hermitian conjugates. As a result, the network can be simplified and acquires the triangular shape shown in Fig. 1 (c) [10, 12].

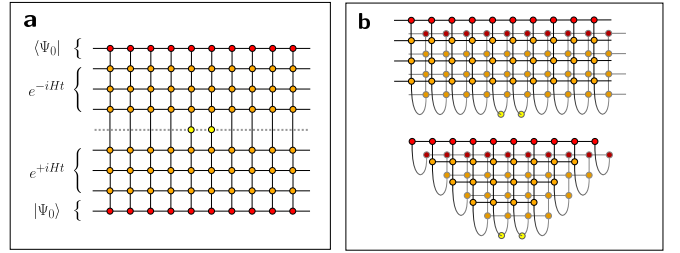


FIG. 1. (a) The time-dependent expectation value of a local operator acting on a one-dimensional system in the Keldysh representation is described by a double sheet 2D tensor network contraction. (b) Upon using a Trotter approximation and the locality of the operator the tensor network simplifies to a triangular TN.

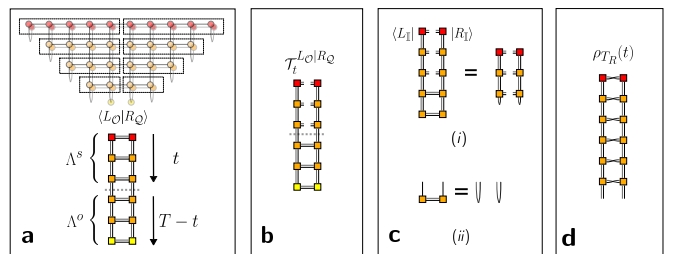


FIG. 2. (a): The triangular tensor network can be contracted from the sides, identifying a left $\langle L_{\mathcal{O}} |$ and a right $| R_{\mathcal{Q}} \rangle$ tMPS. When contracting along the spatial direction, the bond dimension of the corresponding tMPS tensors grows exponentially, so that some truncation is necessary. The upper-most tensors of the temporal MPS are dictated by the initial state $|\psi_0\rangle$ while the lower-most ones by the choice of the operator \mathcal{O} . (b) The reduced transition matrix. (c) In the absence of a local operator, the folded tensors of the time evolution resolve to identities. (d) The partial transpose of the time-evolved left-right density matrix of the system, where forwards and backwards legs are swapped.

The temporal MPS. One strategy to contract this tensor network is to identify two temporal MPS (tMPS), defining the contraction of the left half and the right half of the system (see Fig. 2), and interpret the triangular network as the scalar product between the two,

$$\langle \mathcal{O}\mathcal{Q} \rangle(t) = \langle L_{\mathcal{O}} | R_{\mathcal{Q}} \rangle. \quad (2)$$

Notice that this definition differs slightly from those of previous works, since the specific operators $\mathcal{O}\mathcal{Q}$ are included in the definition of the tMPS.

In practice, the identification is purely formal since as explicitly shown in Fig. 2, the bond dimension of the individual tMPS tensors can grow exponentially with the number of time steps, similarly to what happens for the bond dimension of the standard MPS that describe the evolution of the state $|\psi(t)\rangle$. The construction of the tMPS thus only makes sense if we can show that at least for specific scenarios the tMPS bond dimension increases mildly with the number of time steps.

Compressing the tMPS. In order to understand the properties of the tMPS we start by observing that, by construction, if we chose as two-sites operators the identity operator, $\mathcal{O}\mathcal{Q} = \mathbb{I}$ we obtain that

$$\langle L_{\mathbb{I}} | R_{\mathbb{I}} \rangle = \langle \psi(t) | \psi(t) \rangle = 1. \quad (3)$$

As observed in [6] and exploited in [15] in the $\delta t \rightarrow 0$ limit, both $\langle L_{\mathbb{I}} \rangle$ and $|R_{\mathbb{I}}\rangle$ are described by continuous MPS [31]. This is something we will not use here, since we aim at investigating the complexity of simulating time evolution at fixed δt for long times T , which typically comes into play when addressing problems such as thermalization or generalized-thermalization [32–35].

Given that the bond dimension of the tMPS matrices can in principle increase exponentially with the number of Trotter steps, we need to find a way to identify the relevant rank of those matrices and compress them on their support. The relevant rank is dictated by the physical properties that we want to describe. By choosing to work with a tMPS formulation, we are implicitly suggesting we are only interested in arbitrary correlation functions of the type $\langle \mathcal{O}\mathcal{P}(t) \cdots \mathcal{Q}\mathcal{R}(t') \rangle$ for an arbitrary number of insertions of local operators at different times between 0 and T . Following the standard DMRG recipe [25], this requires having a faithful representation of all reduced-transition matrices (RTM),

$$\mathcal{T}_t^{L_{\mathcal{O}}|R_{\mathcal{Q}}} = \text{tr}_{T-t} \left[\mathcal{T}^{L_{\mathcal{O}}|R_{\mathcal{Q}}} \right], \quad (4)$$

which can be seen as generalizations of reduced density matrices. For the case of interest, rather than dealing with partial traces of the density matrix we thus have to deal with partial traces of the transition matrix defined by

$$\mathcal{T}^{L_{\mathcal{O}}|R_{\mathcal{Q}}} = \frac{|R_{\mathcal{Q}}\rangle \langle L_{\mathcal{O}}|}{\langle L_{\mathcal{O}} | R_{\mathcal{Q}} \rangle}. \quad (5)$$

The graphical representation of these objects is found in Fig. 2(b).

Interestingly, such transition matrices have also been considered in the context of holography, where the duality transformation between a field theory described on the boundary and the theory of gravity in the bulk is studied. The properties of the equivalent in the field theory of the transition matrices described here have a geometrical interpretation in the bulk [36–39].

As a result, the rank of the tMPS matrices is not dictated by the temporal entropy considered previously [4, 6, 10, 12], but rather by the rank of the RTM. Generalizing the standard DMRG prescription, the bond dimension of the tMPS tensors should allow to obtain a low-rank approximation of the reduced transition matrix with the desired precision. As a consequence, the tMPS matrices are compressed by enforcing that they provide the correct low rank approximations of $\mathcal{T}_t^{L_{\mathcal{O}}|R_{\mathcal{Q}}}$, $\forall t \in 0 \dots T$.

Notice that the reduced transition matrices are complex valued, and that whenever $\mathcal{Q} = \mathcal{O}$ they are symmetric. As a result, their low rank approximation is better defined in terms of their singular values, namely we will project the tMPS bond dimension at time t on the largest singular values of $\mathcal{T}_t^{L_{\mathcal{O}}|R_{\mathcal{Q}}}$.

Following [6], we now define $\Lambda^s(t)$ and $\Lambda^o(t)$ respectively as the contractions of the overlap $\langle L_{\mathcal{O}} | R_{\mathcal{Q}} \rangle$ until t (the top part of the network contraction, including the initial state) and below t (the bottom part, containing the operator), respectively, see Fig. 2. We also define $\bar{\Lambda}_L^s(t)$, $\bar{\Lambda}_R^s(t)$ as the contraction up to t of the network obtained by contracting $\langle L_{\mathcal{O}} | L_{\mathcal{O}} \rangle$ and $\langle R_{\mathcal{Q}} | R_{\mathcal{Q}} \rangle$.

With these definitions, we have that

$$\mathcal{T}_t^{L_{\mathcal{O}}|R_{\mathcal{Q}}} \simeq \sqrt{\bar{\Lambda}_L^s(t)} \Lambda^o(t) \sqrt{\bar{\Lambda}_R^s(t)}, \quad (6)$$

where we use the similarity symbol to indicate that the two operators share the same singular values (see Appendix). For reflection invariant systems, such as those we analyze here, one has $\bar{\Lambda}_R^s(t) = \bar{\Lambda}_L^s(t)$, thus our central result reads

$$\mathcal{R} \left(\mathcal{T}_t^{L_{\mathcal{O}}|R_{\mathcal{Q}}} \right) \leq \min \{ \mathcal{R} (\bar{\Lambda}_L^s(t)), \mathcal{R} (\Lambda^o(t)) \}, \quad (7)$$

where \mathcal{R} denotes the rank of a given matrix. This equation is at the basis of our analysis of the numerical complexity of computing the time-evolution of local observables by folding the 2D tensor network and contracting the corresponding tMPS.

Our algorithm constructs a different MPS representation of $\langle L_{\mathcal{O}}(t) |$ and $| R_{\mathcal{Q}}(t) \rangle$. It is thus natural to define the cost of the algorithm as the cost of simulating the operators that require the highest bond dimension. We also can consider the cost of evolving the worst initial product state, that is the product state for which the temporal entanglement grows faster.

The rank of reduced transition matrices. Let us now better characterise the objects appearing in the definition of the reduced transition matrices (6).

Whenever $\mathcal{O} = \mathcal{Q} = \mathbb{I}$, the transition matrices $\mathcal{T}_t^{L_{\mathbb{I}}|R_{\mathbb{I}}}$ for all t are projectors. As a result the states $|L_{\mathbb{I}}\rangle$ and $|R_{\mathbb{I}}\rangle$ consist of trivial singlets at the virtual level for any time t , as sketched in Fig. 2 (c), implying that the tMPS matrices have always bond dimension 1, for all t . In order to obtain non-trivial tMPS we thus need to include the operators in the construction of the states, as already anticipated.

From the previous definitions it follows that

$$\Lambda^o(t) = U(t) (\mathcal{O} \otimes \mathcal{Q}) U(t)^\dagger, \quad (8)$$

meaning that $\Lambda^o(t)$ exactly encodes the Heisenberg evolution of the initially localized operator $\mathcal{O}_i \mathcal{Q}_{i+1}$.

$$\Lambda^s(t) = \rho(t) = U(t) |\psi_0\rangle \langle \psi_0| U(t)^\dagger \quad (9)$$

encodes the evolution of the initial state.

At last, for those H that are invariant under reflections with respect to the center of the chain,

$$\bar{\Lambda}_L^s(t) = \bar{\Lambda}_R^s(t) = \rho(t)_{T_R}, \quad (10)$$

where $\rho(t) = U(t) |\psi_0\rangle \langle \psi_0| U^\dagger(t)$ is the time-evolved density matrix of the initial state, and T_R stands for the partial transpose on the semi-infinite right part of the system. This quantity is sketched in Fig. 2 (d).

Since we are evolving a pure state, there are known relations between $\rho_{T_R}(t)$ and $\rho(t)$ [40], and in particular we know that [41, 42],

$$\mathcal{R}(\bar{\Lambda}_R^s(t)) = \mathcal{R}(\Lambda^s(t)). \quad (11)$$

Having identified the factor matrices of the RTMs in Eq. (6), we can now use their physical properties together with Eq. (7) to identify some useful bound on the rank of the tMPS matrices.

Bound on the tMPS matrices rank. We need to identify if there are physical scenarios for which the relation Eq. (7) allows to bound the tMPS rank. A first scenario is that of a local quench. In this case, it is well known that the entropy of the evolved state only increases logarithmically with time, and as a result the rank of $\Lambda^s(t)$ increases at most polynomially [31, 43], and thus using Eq. (7)

$$\mathcal{R}(\mathcal{T}_t^{L_\mathcal{O}|R_\mathcal{Q}}) \leq T^\alpha \quad \forall t \in \{0, T\}. \quad (12)$$

Such a case is possibly not particularly interesting since a similar polynomial cost is obtained also by using standard MPS algorithms.

We thus turn to the more interesting scenario of a global quench. Here we know that $\mathcal{R}(\Lambda^s(t))$ increases exponentially with T as already mentioned. The only hope is thus that for specific models $\mathcal{R}(\Lambda^o(t))$ only increases polynomially with T . If this is the case, we can find a scenario where the tMPS behaves better than the corresponding MPS. Explicitly, we have

$$\mathcal{R}(\Lambda^o(t)) \leq t^\alpha \Rightarrow \mathcal{R}(\mathcal{T}_t^{L_\mathcal{O}|R_\mathcal{Q}}) \leq T^\alpha \quad \forall t \in \{0, T\}. \quad (13)$$

In this specific case, the temporal MPS strategy provides a polynomial algorithm to compute the out-of-equilibrium dynamics of local observables as already anticipated in [10, 12]. In the literature, it is conjectured (and checked in several scenarios) that in the case of integrable systems the operator entanglement of local operators only grows logarithmically [19–23], implying that the rank of $\Lambda^o(t)$ only increases polynomially with T as required in Eq. (13). As a result, if the conjecture is correct, the tMPS provides an efficient method to characterise the time evolution of local operators for integrable systems.

Since generically the rank of $\Lambda^o(t)$ is expected to grow exponentially with t , we expect that

$$\mathcal{R}(\mathcal{T}_t^{L_\mathcal{O}|R_\mathcal{Q}}) \leq \alpha \exp(\beta), \quad (14)$$

with α and $\beta > 0$ model-dependent constants. In this case, there is no guarantee that the tMPS provides an efficient compression for the problem at hand.

Numerical results. In this section we report the numerical evidence obtained with such an algorithm to support our claims. We consider a transverse field Ising Hamiltonian

$$H(g, h) = - \sum_i \left[\sigma_x^i \sigma_x^{i+1} + g \sigma_z^i + h \sigma_x^i \right], \quad (15)$$

where $\sigma_{x,z}$ are Pauli matrices. We perform a second-order Trotter expansion of the time evolution operator and cast it into an MPO following [30], with a timestep $\delta t = 0.05$. For our examples we consider two cases: an integrable one for $g = 0.5, h = 0$, and a non-integrable one $g = -1.05, h = 0.5$. We consider different initial product states, namely $|0\rangle = (1, 0)^{\otimes N_x}$, $|+\rangle = (1, 1)/\sqrt{2}^{\otimes N_x}$ and $|r\rangle = (1, i)/\sqrt{2}^{\otimes N_x}$ in the z basis.

The time evolution is performed by a variant of the standard folding algorithms that exploit the causal-cone of the network [4, 6, 10, 12] and relies on a low-rank approximation of the RTMs defined in Eq. (4).

As in previous approaches [10, 12] we iteratively construct the left and right vectors $\langle L_\mathcal{O}(T)|$ and $|R_\mathcal{Q}(T)\rangle$ starting from $\langle L_\mathcal{O}(T-1)|$ and $|R_\mathcal{Q}(T-1)\rangle$ by absorbing a new column of MPOs into them. These MPOs are obtained by contracting a column of the original tensor network and they thus represent transfer matrices \mathbb{E}^T evolving states of a time-slice in space, a *rotated* version of the standard evolution in time. The bond dimension of the corresponding MPS increases, and we then keep it under control by projecting onto the largest χ singular values of $\mathcal{T}_t^{L_\mathcal{O}|R_\mathcal{Q}}$ for every bi-partition of the system into t and $T-t$. Further details about the algorithm and accurate comparison with other folding algorithms in the literature are presented in the accompanying Appendix.

In the case of the Ising model, we found the operator with the largest bond dimension defined at most on two sites to be a single-site σ_x . In the following we will focus on optimizing with respect to it [44].

We start by considering the bond dimension necessary to keep the truncation error above a threshold $\epsilon = 10^{-4}$ in the SVD spectrum of the reduced transition matrices, and compare them with those obtained imposing the same truncation on the Heisenberg evolution for the operator $O(t)$, which entails the evolution of the vectorized local operator under the Hamiltonian $H \otimes \mathbb{I} - \mathbb{I} \otimes H$, resulting in the MPS, $|\psi_O(t)\rangle$. The results are shown in Fig. 3, where we can observe that, as expected: 1) the behavior is different in the integrable and non-integrable

cases, 2) the bond dimension necessary to correctly describe the RTM are always below the ones necessary to describe the Heisenberg evolution of the operator. In the integrable case, this bond dimension only increases polynomially (straight line in log-log plot) in time.

We would then be tempted to infer that the computational cost of simulating the expectation value of local operators with a finite precision using a tMPS is upper-bounded by the one of computing the Heisenberg evolution of the same operator. Unfortunately this is not the case, since in order to compute that computational cost we need to determine the bond dimension that is required in order to keep the distance in norm $\|\langle L_{\mathcal{O}} \rangle - \langle L_{\mathcal{O}}^D \rangle\|^2$ constant, where $\langle L_{\mathcal{O}}^D \rangle$ is the truncation of the tMPS $\langle L_{\mathcal{O}} \rangle$ to a given bond dimension D . Using the reasoning in Ref. [31], the term we need to consider would then be the overlap $\langle L_{\mathcal{O}} | L_{\mathcal{O}}^D \rangle$, which is upper bounded by the sum of the norm of the residuals discarded in the truncation process.

So far we have just provided a bound on the overlap $\langle L_{\mathcal{O}} | R_{\mathcal{O}} \rangle$ which, even for reflection invariant systems and considering the symmetric case $\mathcal{O} = \mathcal{Q}$, differs from $\langle L_{\mathcal{O}} | L_{\mathcal{O}}^D \rangle$ by the absence of a complex conjugation. However, we can see that the two quantities are related, since $\langle L_{\mathcal{O}} | L_{\mathcal{O}}^D \rangle$ can be obtained from $\langle L_{\mathcal{O}} | R_{\mathcal{O}} \rangle$ by evolving $|R_{\mathcal{O}}\rangle$ with one layer of local unitaries, representing the partial transpose (a swap evolution between the bra and the ket legs). Such an operation, given the Lieb-Robinson bounds, can at most add a constant amount of entanglement to $|R_{\mathcal{O}}\rangle$ while mapping it to $|L_{\mathcal{O}}^D\rangle$.

As a result, the computational cost required for simulating the expectation value of a local operator with a finite precision independent on the time using a tMPS is constantly offset from the cost of computing $\langle L_{\mathcal{O}} | R_{\mathcal{O}} \rangle$, the latter being upper bounded by the cost of the Heisenberg evolution of the operator. It follows that the scaling in time of the cost to maintain a constant error in local observables, which ultimately is what determines the computational complexity of $\langle L_{\mathcal{O}} | L_{\mathcal{O}}^D \rangle$, is the same as the one of $\langle L_{\mathcal{O}} | R_{\mathcal{O}} \rangle$ (see also the discussion comparing different optimization methods in the Appendix).

We verify this explicitly by following a procedure similar to the one employed in [19] to estimate the truncation error in our tMPS compared to an exact result, which in our case corresponds to the evolution obtained with the maximum bond dimension we can afford, $D_{\max} (\simeq 1000)$. The largest T we consider for this estimation are thus restricted to times for which D_{\max} does not induce any sizeable truncation error with respect to the exact (Trotterized) dynamics. If we work with normalized MPS, the error induced by truncating the operator MPS to bond dimension D is encoded in the fidelity $F = |\langle \psi_{\mathcal{O}}^{D_{\max}}(t) | \psi_{\mathcal{O}}^D(t) \rangle|$, where $|\psi_{\mathcal{O}}^D(t)\rangle$ represents the time-evolved state up to time t truncated at every time step to bond dimension D . By fixing a given accuracy ϵ , we thus identify the maximum time for which $F \geq 1 - \epsilon$.

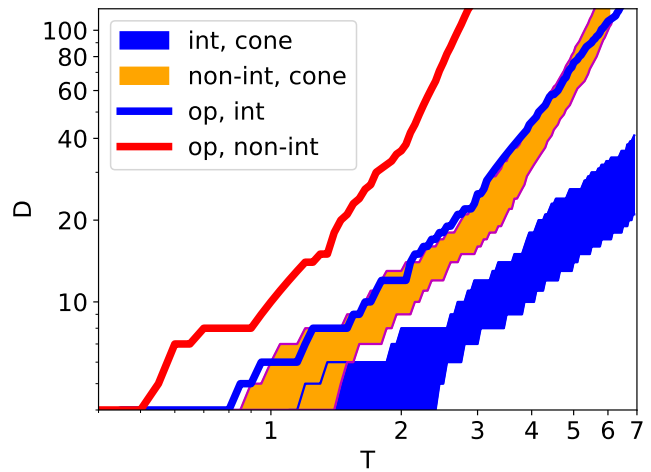


FIG. 3. Bond dimensions D obtained imposing a truncation error of 10^{-4} in the SVD of the RTMs, as a function of time. The shaded areas are delimited by the minimum and maximum bond dimension found by varying the initial state (among the product states we considered, $|0\rangle$ gives the largest result, $|+\rangle$ the lowest) for the integrable (blue) and non-integrable (orange) case. The corresponding operator entanglement bond dimension curves are shown as solid lines: they lie consistently above the corresponding ones for the tMPS.

As a consequence, by repeating the above procedure for different D we can identify a curve $D^*(t)$ along which the truncation error is kept roughly constant at a value ϵ .

We then extract a similar curve $D^*(t)$ for the tMPS encoding the semi-infinite left (right) tensor network $\langle L_{\mathcal{O}} | (|R_{\mathcal{O}}\rangle)$. The truncation here is based on projecting onto the largest singular values of each RTM, as described above. The largest D_{\max} we can afford is again used as the exact reference. The overlap of the two tMPS measures the effects of the truncation error $F = |\langle L_{\mathcal{O}}^{D_{\max}} | L_{\mathcal{O}}^D \rangle|$. Once more by fixing such an error to a given threshold ϵ we can identify the corresponding $D^*(t)$ for the tMPS. The typical behavior of the resulting curves for F can be seen in Fig. 4.

The resulting D^* are reported in Fig. 5. For the integrable case, we find a polynomial increase of the bond dimension of the tMPS, consistent with the behavior of the operator entanglement. Different initial states require different bond dimensions for a faithful description, though the growth follows the same power law. For the non-integrable case the behavior is different: as is well known [19], the operator entanglement requires an exponentially growing bond dimension for a faithful description, and the tMPS bond dimension follows the same behavior, consistent with our result.

As expected the slope of the curves for maintaining a fixed error in simulating local observables with tMPS is the same than the slope of the curve required to simulate the Heisenberg evolution with a constant error.

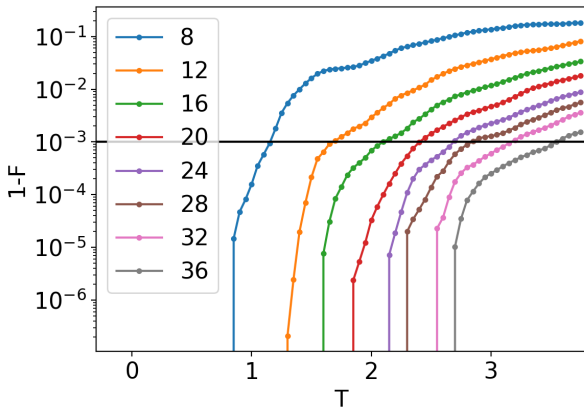


FIG. 4. Fidelity for overlap $\langle L_{\mathcal{O}}^{D_{\max}} | L_{\mathcal{O}}^D \rangle$ for different bond dimensions, as function of time, for the integrable case with starting state $|+\rangle$. After fixing a threshold ϵ we can extract the required bond dimension to give a faithful approximation of $|L_{\mathcal{O}}^D\rangle$.

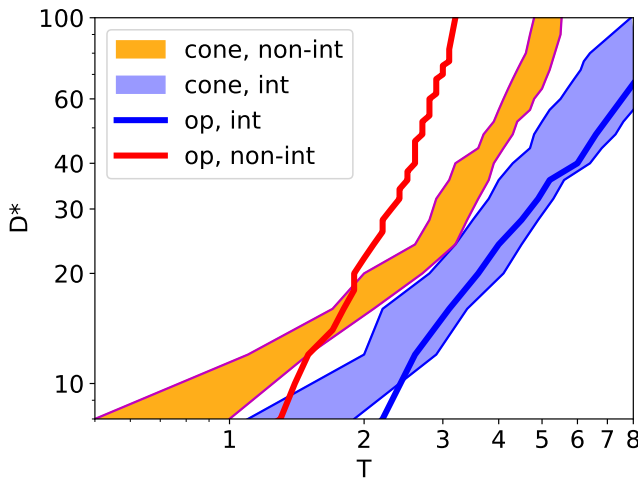


FIG. 5. Bond dimensions D^* obtained by imposing a fidelity of $5 * 10^{-3}$ on the fidelity for $\langle L_{\mathcal{O}} \rangle$, (represented again in bands delimited by the highest and lowest values obtained by changing the initial state), compared with the corresponding operator entanglement (solid lines). Blue lines represent the integrable model, red the non-integrable case.

Conclusions. We have provided a new connection between two separate concepts, temporal entanglement and the operator entanglement. In particular, we have shown that the rank of the RTM necessary to compute the temporal entanglement is upper bounded by the rank of the operator entanglement of a bi-partition. As a result, the scaling in time of the computational cost of simulating the evolution of a local observable with constant error is upper-bounded by the scaling of the operator entanglement, even though the exact value of the cost can be

offset by a constant value whose origin has been discussed in detail.

As a result, we can claim that whenever the operator entanglement only grows polynomially, using a tMPS for simulating the evolution of a local observable is the best choice in terms of computational cost and scales only polynomially with time. Our presented algorithm yields the most efficient performance observed thus far, with a marginal advantage over previous approaches.

Our results are a step towards understanding the cost of simulating the out-of-equilibrium dynamics of quantum many-body systems. It would be interesting to check the bounds we have obtained on a larger class of integrable and non-integrable models, and more importantly to explore if the transverse contraction can help in simulating the dynamics of higher dimensional systems.

While working on this paper, we found out about Ref. [45] working on similar issues and suggesting a connection between the operator entanglement and the temporal entanglement, a connection we hope to have elucidated with our work.

Acknowledgements: We acknowledge the precious discussions on this and related subjects with Mari-Carmen Bañuls, Miguel Frías-Pérez, Dmitry Abanin, Tomaž Prosen, Ignacio Cirac, Pavel Kos, Jan Schneider and Georgios Styliaris. LT acknowledges support from the Proyecto Sinérgico CAM 2020 Y2020/TCS-6545 (NanoQuCo-CM), the CSIC Research Platform on Quantum Technologies PTI-001 and from Spanish projects PID2021-127968NB-I00 and TED2021-130552B-C22 funded by MCIN/AEI/10.13039/501100011033/FEDER, UE and MCIN/AEI/10.13039/501100011033, respectively.

* stefano.carignano@bsc.es

† luca.tagliacozzo@iff.csic.es

- [1] M. Qin, T. Schäfer, S. Andergassen, P. Corboz, and E. Gull, *Annual Review of Condensed Matter Physics* **13**, 275 (2022).
- [2] P. Calabrese and J. Cardy, *J. Stat. Mech.* **2005**, P04010 (2005).
- [3] A. Laeuchli and C. Kollath, *J. Stat. Mech.* **2008**, P05018 (2008), arxiv:0803.2947 [cond-mat].
- [4] M. C. Bañuls, M. B. Hastings, F. Verstraete, and J. I. Cirac, *Phys. Rev. Lett.* **102**, 240603 (2009).
- [5] A. Müller-Hermes, J. I. Cirac, and M. C. Bañuls, *New J. Phys.* **14**, 075003 (2012), arxiv:1204.5080 [cond-mat, physics:quant-ph].
- [6] M. B. Hastings and R. Mahajan, *Phys. Rev. A* **91**, 032306 (2015), arxiv:1411.7950 [cond-mat, physics:hep-th, physics:quant-ph].
- [7] A. Strathearn, P. Kirton, D. Kilda, J. Keeling, and B. W. Lovett, *Nat Commun* **9**, 3322 (2018).
- [8] C. D. White, M. Zaletel, R. S. K. Mong, and G. Refael, (2017), arxiv:1707.01506.

[9] T. Rakovszky, C. W. von Keyserlingk, and F. Pollmann, *Dissipation-assisted operator evolution method for capturing hydrodynamic transport* (2020), [arxiv:2004.05177 \[cond-mat\]](https://arxiv.org/abs/2004.05177).

[10] M. Frías-Pérez and M. C. Bañuls, *Phys. Rev. B* **106**, 115117 (2022), [arxiv:2201.08402 \[quant-ph\]](https://arxiv.org/abs/2201.08402).

[11] A. Lerose, M. Sonner, and D. A. Abanin, *Phys. Rev. X* **11**, 021040 (2021).

[12] A. Lerose, M. Sonner, and D. A. Abanin, *Phys. Rev. B* **107**, L060305 (2023).

[13] G. Giudice, G. Giudici, M. Sonner, J. Thoenmiss, A. Lerose, D. A. Abanin, and L. Piroli, [arxiv:2112.14264 \[cond-mat, physics:quant-ph\]](https://arxiv.org/abs/2112.14264) (2021), [arxiv:2112.14264 \[cond-mat, physics:quant-ph\]](https://arxiv.org/abs/2112.14264).

[14] J. Thoenmiss, A. Lerose, and D. A. Abanin, *Physical Review B* **107**, 195101 (2023).

[15] E. Tirrito, N. J. Robinson, M. Lewenstein, S.-J. Ran, and L. Tagliacozzo, *Characterizing the quantum field theory vacuum using temporal Matrix Product states* (2022), [arxiv:1810.08050 \[cond-mat\]](https://arxiv.org/abs/1810.08050).

[16] R. Feynman and F. Vernon, *Annals of Physics* **24**, 118 (1963).

[17] M. Sonner, A. Lerose, and D. A. Abanin, *Annals of Physics Special Issue on Philip W. Anderson*, **435**, 168677 (2021).

[18] E. Ye and G. K.-L. Chan, *J. Chem. Phys.* **155**, 044104 (2021), [arxiv:2101.05466 \[physics, physics:quant-ph\]](https://arxiv.org/abs/2101.05466).

[19] T. Prosen and M. Žnidarič, *Phys. Rev. E* **75**, 015202 (2007).

[20] I. Pižorn and T. Prosen, *Phys. Rev. B* **79**, 184416 (2009).

[21] J. Dubail, *J. Phys. A: Math. Theor.* **50**, 234001 (2017), [arxiv:1612.08630 \[cond-mat, physics:hep-th, physics:quant-ph\]](https://arxiv.org/abs/1612.08630).

[22] B. Bertini, P. Kos, and T. Prosen, *SciPost Physics* **8**, 067 (2020).

[23] B. Bertini, P. Kos, and T. Prosen, *SciPost Physics* **8**, 068 (2020).

[24] G. Vidal, *Phys. Rev. Lett.* **93**, 040502 (2004).

[25] S. R. White and A. E. Feiguin, *Phys. Rev. Lett.* **93**, 076401 (2004).

[26] S. Paeckel, T. Köhler, A. Swoboda, S. R. Manmana, U. Schollwöck, and C. Hubig, (2019), [arxiv:1901.05824 \[cond-mat, physics:quant-ph\]](https://arxiv.org/abs/1901.05824).

[27] M. C. Bañuls, *Annual Review of Condensed Matter Physics* **14**, 173 (2023).

[28] This can be easily generalized to an arbitrary number of sites as long as it is finite.

[29] I. P. McCulloch, *Journal of Statistical Mechanics: Theory and Experiment* **2007**, P10014 (2007).

[30] B. Pirvu, V. Murg, J. I. Cirac, and F. Verstraete, *New Journal of Physics* **12**, 025012 (2010).

[31] F. Verstraete and J. I. Cirac, *Phys. Rev. Lett.* **104**, 190405 (2010).

[32] M. Rigol, V. Dunjko, V. Yurovsky, and M. Olshanii, *Physical Review Letters* **98**, 10.1103/PhysRevLett.98.050405 (2007).

[33] A. Polkovnikov, K. Sengupta, A. Silva, and M. Vengalattore, *Reviews of Modern Physics* **83**, 863 (2011).

[34] L. Vidmar and M. Rigol, *Journal of Statistical Mechanics: Theory and Experiment* **2016**, 64007 (2016).

[35] C. Gogolin and J. Eisert, *Reports on Progress in Physics* **79**, 056001 (2016).

[36] Y. Nakata, T. Takayanagi, Y. Taki, K. Tamaoka, and Z. Wei, *Phys. Rev. D* **103**, 026005 (2021), [arxiv:2005.13801 \[cond-mat, physics:hep-th, physics:quant-ph\]](https://arxiv.org/abs/2005.13801).

[37] K. Doi, J. Harper, A. Mollabashi, T. Takayanagi, and Y. Taki, *Timelike entanglement entropy* (2023), [arxiv:2302.11695 \[cond-mat, physics:hep-th, physics:quant-ph\]](https://arxiv.org/abs/2302.11695).

[38] K. Narayan and H. K. Saini, *Notes on time entanglement and pseudo-entropy* (2023), [arxiv:2303.01307 \[hep-th\]](https://arxiv.org/abs/2303.01307).

[39] X. Jiang, P. Wang, H. Wu, and H. Yang, *Timelike entanglement entropy and $\$T\backslash bar\{T\}\$$ deformation* (2023), [arxiv:2302.13872 \[hep-th\]](https://arxiv.org/abs/2302.13872).

[40] A. Coser, E. Tonni, and P. Calabrese, *J. Stat. Mech.* **2014**, P12017 (2014).

[41] P. Calabrese, J. Cardy, and E. Tonni, *Phys. Rev. Lett.* **109**, 130502 (2012), [arxiv:1206.3092 \[cond-mat, physics:hep-th, physics:quant-ph\]](https://arxiv.org/abs/1206.3092).

[42] G. Vidal and R. F. Werner [10.48550/ARXIV.QUANT-PH/0102117](https://arxiv.org/abs/0102117) (2001).

[43] P. Calabrese and J. Cardy, *Journal of Statistical Mechanics: Theory and Experiment* **2007**, P10004 (2007).

[44] For operators with known small bond dimension such as σ_z or $\sigma_x\sigma_x$, our algorithm saturates at the expected fixed value of D [46].

[45] A. Foligno, T. Zhou, and B. Bertini, *Temporal Entanglement in Chaotic Quantum Circuits* (2023), [arxiv:2302.08502 \[cond-mat, physics:hep-th, physics:math-ph, physics:quant-ph\]](https://arxiv.org/abs/2302.08502).

[46] M. J. Hartmann, *Phys. Rev. Lett.* **102**, 10.1103/PhysRevLett.102.057202 (2009).

[47] This particular choice ensures that the RTM is symmetric, which guarantees that its diagonalization is not an ill-posed problem.

[48] R. Orús and G. Vidal, *Physical Review B* **78**, 155117 (2008).

[49] G. Evenbly [10.48550/ARXIV.2202.02138](https://arxiv.org/abs/10.48550/ARXIV.2202.02138) (2022).

The algorithm

In this Appendix we describe the algorithms we employ to obtain the left and right tMPS encoding the contraction of the tensor network associated with the expectation value $\langle \mathcal{O}(T) \rangle$, where \mathcal{O} is a local operator acting on one or few neighbouring sites. In practice, for the iterative methods we employ it is convenient to incorporate the operator on one side of the network, as will become clear in the following. If we choose eg. to incorporate \mathcal{O} on the right side of the network, our algorithms allow to build $\langle L_{\mathbb{I}} \rangle$ and $|R_{\mathcal{O}}\rangle$ for a given time T .

The basic building blocks of the TN are the MPO tensors representing the trotterized time evolution (here we employ the parametrization from [30]). For a given T which determines the extension of the network in the temporal direction ($N_T = T/\delta t$), we contract them in columns to generate the transfer matrices encoding the rotated (space-like) evolution \mathbb{E}^T for the folded system of which $\langle L |$ and $|R \rangle$ are the leading left and right eigenvectors in the thermodynamic limit. Depending on what we want to construct, we can also include the local operator at the bottom of the transfer matrix, in that case

we label it as $\mathbb{E}_{\mathcal{O}}^T$.

We have implemented both a power-method for extracting the leading eigenvectors of \mathbb{E}^T for a fixed time T , as well as an algorithm based on the strict causal cone of the network when dealing with local operators. Both our algorithms are small variations of those presented in [4, 10, 12]), the main difference being the cost-function we use to perform the truncation required in the various iterations: we project the tMPS matrices on the support of the largest singular values of the respective RTM, as will be explained in the following.

The *power method* (see Fig. 6(a)) works by repeatedly applying the transfer matrix to an initial guess tMPS until convergence is reached. More specifically, we start from the left $\langle L_{\mathbb{I}} \rangle$ and right $|R_{\mathbb{I}}\rangle$ vectors, and apply a column \mathbb{E}^T to the left and a $\mathbb{E}_{\mathcal{O}}^T$ to the right. At each step, the bond dimension of the tMPS increases by a factor d^2 , where d is the physical dimension of the system constituents, so in order to proceed we truncate following our prescription and take the updated $\langle L_{\mathbb{I}} \rangle$ as input for the next step. With our parametrization of the MPO tensors, \mathbb{E}^T is symmetric in left-right legs, so we can use $\langle L_{\mathbb{I}} \rangle$ also as the new $|R_{\mathbb{I}}\rangle$. Alternatively, the optimization for $|R_{\mathbb{I}}\rangle$ simply requires an analogous step involving $|L_{\mathcal{O}}\rangle$.

In order to determine whether the power method has converged, we calculate several entropies associated with the $\langle L_{\mathbb{I}} \rangle$ and $|R_{\mathcal{O}}\rangle$ vectors: most notably, we compute the Von Neumann entropy $S_t^{VN}(L_{\mathbb{I}})$ and the generalized Rényi 2, which we define as $S_t^{r2}(R_{\mathcal{O}}) = -\log \sum_n \lambda_n^2$, where λ_n^2 are the eigenvalues of the RTM $\mathcal{T}_t^{L_{\mathcal{O}}|R_{\mathcal{O}}}$ [47]. Convergence is reached at a given step i of the power method if, for the aforementioned entropies, one has $\sum_{t=0}^{N_T} (S_t^{i-1} - S_t^i)^2 < \epsilon$, which in our case we take to be $\epsilon = 10^{-6}$.

The *light-cone method* works in a slightly different way, as it allows to build the tMPS for a time T starting from the one for $T-1$ with a single optimization (see Fig. 6(b)): Starting from $\langle L_{\mathbb{I}} \rangle$ and $|R_{\mathbb{I}}\rangle$ of a given length N_T , we apply a transfer matrix \mathbb{E}^{T+1} of length $N_T + 1$ to the left and a $\mathbb{E}_{\mathcal{O}}^T$ to the right, extending the network both in the time and space direction.

As for the power method, after each iteration the bond dimension of the tMPS grows by a factor d^2 , so that truncating is required to avoid an exponential computational cost. The truncated $\langle L_{\mathbb{I}} \rangle$ and $|R_{\mathbb{I}}\rangle$ are then used as starting point for the next iteration. The cone is then built from the center moving outwards, assuming that the truncation of its edges does not spoil the causal structure induced by the local operator. The algorithm seems in any case to be quite stable, as we checked by piling up periodically a few layers of \mathbb{E}^T before truncating and verifying that the final result is the same as the one obtained when we truncate after each iteration.

In spite of their differences, both methods end up giving comparable results, as they share the same truncation

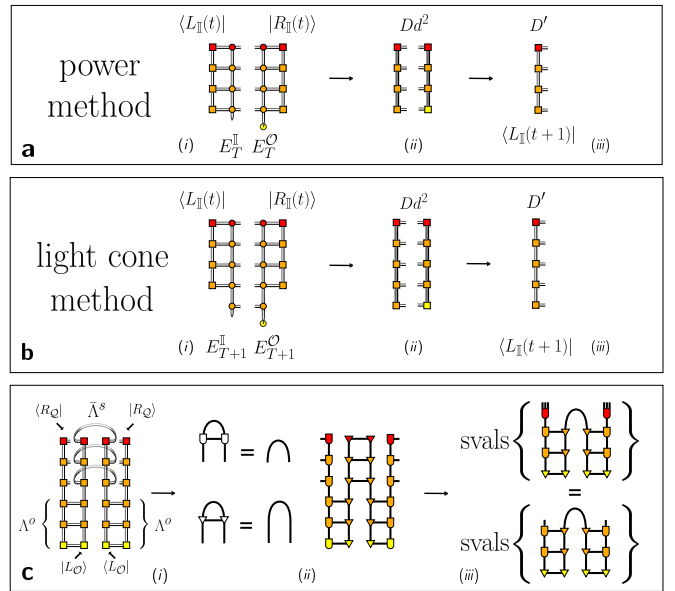


FIG. 6. Illustrations of the methods used for building the tMPS. (a) Power method (b) Light cone method (c) The matrix involved in our low-rank approximation of \mathcal{T} and the role of the gauge transformation in our calculation.

procedure, which goes as follows: We focus on optimizing the overlap between $\langle L_{\mathbb{I}} \rangle$ and $|R_{\mathcal{O}}\rangle$, which includes the operator whose expectation value we are interested in. Since our aim is to find a low-rank approximation for the RTM $\mathcal{T}_t^{L_{\mathbb{I}}|R_{\mathcal{O}}}$ at any bi-partition t and $T-t$, we consider the eigenvalues of the matrix $(\mathcal{T}_t^{L_{\mathbb{I}}|R_{\mathcal{O}}})^\dagger \mathcal{T}_t^{L_{\mathbb{I}}|R_{\mathcal{O}}}$ depicted in Fig. 6(c), which can be associated with the squares of the relevant singular values. As usual in TN calculations, we can transform a global optimization problem into a local one by making use of gauge transformation [48, 49]. In particular, we start by bringing both L and R vectors individually to a standard orthogonal gauge, starting from the side of the initial state (Fig. 6 (c)). This gauge transformation allows to incorporate the $\tilde{\Lambda}_{L,R}^s(t)$ factors towards the operator side, so that we don't need to compute them explicitly as their contraction up to $t < T$ now reduces to an identity. We now only need to contract the bottom environments and project them over their largest D' singular values at each t , thus optimizing the overlap between the two tMPS. The advantage of keeping the local operators on one side of the network is that, while we optimize with respect to $\langle \mathcal{O} \rangle$, we always end up with a new $\langle L_{\mathbb{I}} | (|R_{\mathbb{I}}\rangle)$ which does not include the operator itself. This tMPS, which is related rather to the time evolution of the state, thus encodes the influence functional of the system, and can be used as starting point for the next iteration of our algorithms.

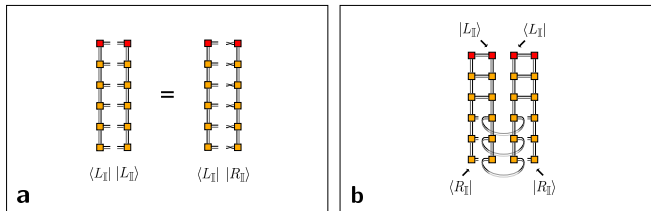


FIG. 7. (a) A possible method for truncating the tMPS relies on the optimization of the overlap $\langle L|L \rangle$, where in the symmetric case $|L\rangle$ can be related by a partial transpose to the vector $|R\rangle$. (b) Alternatively, it is also possible to consider the RTM starting from the side of the initial state, a procedure which can give a nontrivial SVD spectrum even in the absence of a local operator.

Comparison with other approaches

As previously mentioned, our optimization prescription is a relatively small modification with respect to already existing algorithms, which allows nevertheless to make a clearer connection with the underlying structures and estimate the computational complexity associated with the calculation of time-dependent expectation values. It might nevertheless be interesting to check how this method compares with other prescriptions employed in the literature.

The most straightforward optimization procedure when dealing with (t)MPS after applying a column of MPO is to truncate using the standard canonical forms for the left and right vectors separately. In our framework, with left-right symmetry of the Hamiltonian and translational invariance, this would amount to an optimization of $\langle L|$ with its conjugate $|L\rangle$ instead of $|R\rangle$. The operation of complex conjugation here can be seen as a partial transpose involving the forwards and backwards leg of the tMPS (basically an insertion of a series of swap operators), see Fig. 7 (a), since (not considering additional complications in case the initial state is complex) it basically amounts to an exchange $U(t) \leftrightarrow U^\dagger(t)$ of the time evolution operators. Due to the non-trivial structure induced by this, the projector structure of the tensor network is lost even if no operators are present, so that one obtains a non-trivial bond dimension even when $\mathcal{O} = \mathbb{I}$.

Instead of optimizing with respect to a single operator inserted at the edge of the MPO column, the conjugation would imply acting on the whole column, ie. to perform these transpositions at each timestep.

Another possible strategy, which has been suggested in [6, 10] involves bringing the tMPS to canonical form starting from the bottom side and then doing a sweep from the initial state optimizing $\langle L_I|R_I \rangle$, Fig. 7 (b).

In this case, while the spectrum of the RTM is trivial since no operator is present, the singular value decomposition is not: this can be seen again as due to an insertion

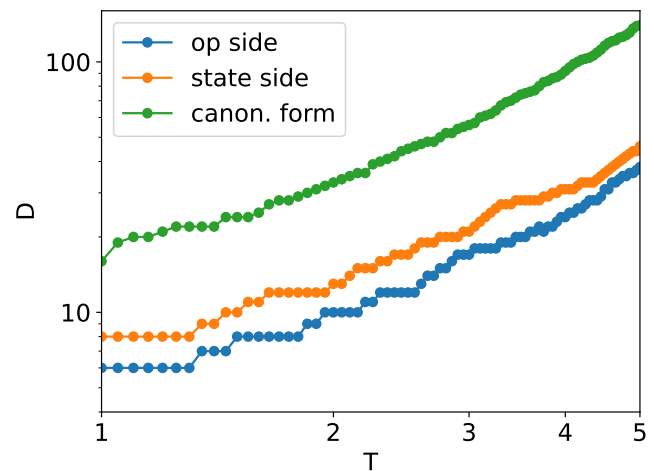


FIG. 8. Bond dimensions of the tMPS as function of time obtained with different methods (as described in the text): our method (blue line), the optimization starting from the side of the initial state (orange) and the canonical form (green), imposing the same truncation error ($\epsilon_{trunc} = 10^{-6}$). Our method leads to the smallest bond dimension.

of swap operators which generate a non-trivial spectrum, which however cannot be directly related to the causal structure generated by a local operator. In this case, one is unable to give a priori a statement on the maximum rank required by the algorithm.

In spite of this difference, remarkably this latter method returns comparable bond dimensions to the ones obtained with our method when $\mathcal{O} = \sigma_x$, see Fig. 8. On the other hand, the optimization using the standard canonical forms requires a larger bond dimension, although the behavior of the various algorithms is comparable: this confirms our expectation that the scaling of our truncation based on the overlap $\langle L|R \rangle$ is the same as the one based on $\langle L|L \rangle$.